ADC Nonlinearity Correction for the MAJORANA DEMONSTRATOR

N. Abgrall[1], J. M. Allmond[2], I. J. Arnquist[3], F. T. Avignone III[4,2], A. S. Barabash[5], C. J. Barton[6], F. E. Bertrand[2], B. Bos[7,8], M. Busch[9,10], M. Buuck[11,⋆] , T. S. Caldwell[7,10], C.M. Campbell[1], Y-D. Chan[1], C. D. Christofferson[8], P.-H. Chu[12], M. L. Clark[7,10], H. L. Crawford[1], C. Cuesta[11,†], J. A. Detwiler[11], A. Drobizhev[1], D. W. Edwins[4], Yu. Efremenko[13,2], H. Ejiri[14], S. R. Elliott[12], T. Gilliss[7,10,‡], G. K. Giovanetti[15], M. P. Green[16,10,2], J. Gruszko[7,10], I. S. Guinn[7,10], V. E. Guiseppe[2], C. R. Haufe[7,10], R. J. Hegedus[7,10], R. Henning[7,10], D. Hervas Aguilar[7,10], E. W. Hoppe[3], A. Hostiuc[11], M. F. Kidd[17], I. Kim[12], R. T. Kouzes[3], A. M. Lopez[13], J. M. López-Castaño[6], E. L. Martin[7,10], R. D. Martin[18], R. Massarczyk[12], S. J. Meijer[12], S. Mertens[19,20,11], J. Myslik[1], T. K. Oli[6], G. Othman[7,10], W. Pettus[11], A. W. P. Poon[1], D. C. Radford[2], J. Rager[7,10], A. L. Reine[7,10], K. Rielage[12], N. W. Ruof[11], M. J. Stortini[12], D. Tedeschi[4], R. L. Varner[2], B. R. White[12], J. F. Wilkerson[7,10,2], C. Wiseman[11], W. Xu[6], C.-H. Yu[2], and B. X. Zhu[12,§]

[1]Nuclear Science Division, Lawrence Berkeley National Laboratory, Berkeley, CA 94720, USA
[2]Oak Ridge National Laboratory, Oak Ridge, TN 37830, USA
[3]Pacific Northwest National Laboratory, Richland, WA 99354, USA
[4]Department of Physics and Astronomy, University of South Carolina, Columbia, SC 29208, USA
[5]National Research Center "Kurchatov Institute" Institute for Theoretical and Experimental Physics, Moscow, 117218 Russia
[6]Department of Physics, University of South Dakota, Vermillion, SD 57069, USA
[7]Department of Physics and Astronomy, University of North Carolina, Chapel Hill, NC 27514, USA
[8]South Dakota School of Mines and Technology, Rapid City, SD 57701, USA
[9]Department of Physics, Duke University, Durham, NC 27708, USA
[10]Triangle Universities Nuclear Laboratory, Durham, NC 27708, USA
[11]Center for Experimental Nuclear Physics and Astrophysics, and Department of Physics, University of Washington, Seattle, WA 98195, USA
[12]Los Alamos National Laboratory, Los Alamos, NM 87545, USA
[13]Department of Physics and Astronomy, University of Tennessee, Knoxville, TN 37916, USA
[14]Research Center for Nuclear Physics, Osaka University, Ibaraki, Osaka 567-0047, Japan
[15]Physics Department, Williams College, Williamstown, MA 01267, USA
[16]Department of Physics, North Carolina State University, Raleigh, NC 27695, USA
[17]Tennessee Tech University, Cookeville, TN 38505, USA
[18]Department of Physics, Engineering Physics and Astronomy, Queen's University, Kingston, ON K7L 3N6, Canada
[19]Max-Planck-Institut für Physik, München, 80805 Germany
[20]Physik Department and Excellence Cluster Universe, Technische Universität, München, 85748, Germany

Imperfections in analog-to-digital conversion cannot be ignored when signal digitization requirements demand both wide dynamic range and high resolution, as is the case for the MAJORANA DEMONSTRATOR ^{76}Ge neutrinoless double beta decay search. Enabling the experiment's high-resolution spectral analysis and efficient pulse shape discrimination required careful measurement and correction of ADC nonlinearites. A simple measurement protocol was developed that did not require sophisticated equipment or lengthy data taking campaigns. A slope-dependent hysteresis was observed and characterized. A correction applied to digitized waveforms prior to signal processing reduced the differential and integral nonlinearites by an order of magnitude, eliminating these as dominant contributions to the systematic energy uncertainty at the double-beta decay Q value.

***Index Terms*—germanium detectors, enriched ^{76}Ge, neutrinoless double beta decay, signal processing.**

I. INTRODUCTION

EXPERIMENTS requiring signal digitization with both wide dynamic range and high resolution must pay special attention to nonlinearities in analog-to-digital conversion (ADC). The MAJORANA DEMONSTRATOR [1] is such an experiment, consisting of an array of enriched high-purity germanium detectors used to search for the neutrinoless double-beta ($0\nu\beta\beta$) decay of ^{76}Ge. This hypothetical nuclear decay emits two electrons without the balancing emission of anti-leptons;

⋆ Present address: SLAC National Accelerator Laboratory, Menlo Park, CA 94025, USA
† Present address: Centro de Investigaciones Energéticas, Medioambientales y Tecnológicas, CIEMAT 28040, Madrid, Spain
‡ Present address: Applied Physics Laboratory, Johns Hopkins University, Laurel, MD 20723, USA
§ Present address: Jet Propulsion Laboratory, California Institute of Technology, Pasadena, CA 91109, USA

the observation of such a matter creation process would signify that lepton number is not conserved, with implications for the matter-antimatter asymmetry of the universe [2]. The DEMONSTRATOR requires a wide dynamic range for detection of low-energy spectral features of backgrounds for high-energy $0\nu\beta\beta$ decay signals. A wide dynamic range also enables searches for other Beyond-the-Standard-Model physics at low energy [3], [4]. High resolution is required for efficient pulse shape discrimination (PSD) of gamma and alpha radiation, and for careful measurement of the signal amplitude (energy) to distinguish $0\nu\beta\beta$ decay from the Standard Model process in which two neutrinos are emitted. Recently, the MAJORANA collaboration published its $0\nu\beta\beta$ decay search results [5], [6], demonstrating high-efficiency PSD, very low background, and the best energy resolution to date among large-scale $0\nu\beta\beta$ decay searches. This achievement was made possible in part by the novel method presented in this paper for measuring and correcting ADC nonlinearities in the GRETINA Digitizer Modules [7], [8] employed in the MAJORANA DEMONSTRATOR.

The experiment is staged at the 4850-foot level of the Sanford Underground Research Facility [9] in Lead, SD. It is composed of 58 p-type point contact (PPC) high purity germanium detectors divided between two compact arrays housed within identical low-background cryostats. Each of the two detector arrays contains seven strings, with each string being an assembly of three, four, or five vertically stacked detectors. The PPC technology [10], [11] was selected because of its superb energy resolution and ability to distinguish between multi- and single-site interactions. Charge collection in PPC detectors occurs on time scales of hundreds of nanoseconds to a microseconds [12].

The point contact of the detector is connected by a spring-loaded pin to the gate of a field-effect transistor (FET) mounted on a low-mass front end (LMFE) board made of high-radiopurity materials [13]. In addition to the FET this circuit incorporates an amorphous-Ge feedback resistor, and the proximity of its traces provides the appropriate feedback capacitance for the charge-based amplification of the detector signals. The circuit also includes an additional capacitive-coupled trace for sending test pulses to the gate of the FET. The LMFE is located close to the detector in order to minimize stray input capacitance. The RC constant of the feedback loop is on the order of milliseconds.

The rest of the preamplifier lies outside the cryostat and is connected to the LMFE by a long (2.15 m) length of cable [13]. The voltage at the first stage of the preamplifier is measured at regular intervals to monitor temperature and leakage current stability. The second stage of the preamplifier is AC coupled to the first stage, and has two differential outputs which differ in gain by a factor of $\sim$3. The detector signals have a sharp rising edge, the structure of which provides information on the charge drift, and a tail that falls exponentially with a $\sim$70 μs time constant arising from the AC coupling between the first and second stages of the preamplifier.

For each crystal array, four circuit boards ("controller cards") interface with the preamplifiers. Each of these controller cards contains sixteen 12-bit ADCs for monitoring baseline voltages and sixteen 16-bit digital-to-analog converters (DACs) for pulsing the FETs. The pulsers allow distribution of pulses of programmable amplitude and frequency to specified sets of FETs. These pulsers are used to monitor gain stability, trigger efficiency, and detector livetime. The pulsers can also be used for validation of digitizer linearity, as discussed below.

The high and low gain outputs of each detector's preamplifier are connected to separate digitization channels. The GRETINA Digitizer Modules provide 10 channels per card, each with differential input and a 14-bit ADC digitizing at 100 MHz. The input dynamic range is $\pm$1.25 V. An on-board field-programmable gate array (FPGA) performs digital discrimination and trapezoidal shaping. The digitizers provide various triggering modes and accomplish raw data storage of triggered signals with a FIFO (first in, first out) memory. Signal pre-summing of portions of the waveform allows for the optional extension of the time window captured within the 2000 sample limit for each recorded trace. The digitization electronics for the two cryostats operate out of separate VME crates, each housing the requisite number of GRETINA digitizer boards and a single board computer (SBC) to read out the digitizers in that crate. The two SBCs communicate with one central computer running ORCA (Object Oriented Real-time Control and Acquisition) which controls the entire data acquisition (DAQ) system [14]. All acquisition parameters are programmable and easily accessed through an ORCA interface.

Full analysis of the pulse shapes is performed offline in software. Signal amplitudes are measured to estimate event energies using a trapezoidal filter with a 4 μs integration time, a flat-top of 2.5 μs, and employing a modified pole-zero adjustment to correct for charge trapping [15]. The smoothed derivative of the pulse is computed with a running linear fit over a $\sim$100 ns range to distinguish single-site signal events from multi-site background interactions [16]. A third pulse shape parameter looks for excess slope in the exponential tail of the pulse that indicates the presence of "delayed charge recovery" (DCR) following surface alpha background interactions [17]. These algorithms all rely on linear analog-to-digital conversion of the detector signals.

Periodic nonlinearities have been observed in the ADC chips used in the GRETINA Digitizer Module (Analog Devices AD6645) arising from the subranging nature of the ADC implementation. Of particular note is that the nonlinearities in these ADCs depend not only on the voltage level but also the rate at which the voltage changes [18]. Uncorrected, these ADC nonlinearities affect energy determination by up to several keV and degrade both of the key pulse shape parameters used to reject background events.

A number of methods are available for correcting nonlinearity, for example the histogram method [19], integral nonlinearity curve tables [20], using the analytic inverse of the integral nonlinearity curve [21], and the blind calibration algorithm [22]. However, most methods require special equipment or architectures, and/or lengthy measurement campaigns. They also often assume that ADC differential nonlinearities are fixed constants that are independent of the time variation of the

input signal. These aspects made standard methods inadequate for the MAJORANA DEMONSTRATOR.

In this paper, we present the nonlinearity correction developed for the MAJORANA DEMONSTRATOR. First we will describe the measurement of the nonlinearities by applying external signals and measuring the response of each digitizer channel. Then we describe our nonlinearity correction algorithm, and quantify the energy performance of the DEMONSTRATOR after applying the nonlinearity correction. Finally, we discuss the validation of the linearity of the corrected energy spectrum using external pulsers.

II. NONLINEARITY MEASUREMENT

Our measurement of ADC nonlinearity is performed through application of summed ramped voltage signals sent directly to the front-end inputs of a digitizer. With linearly ramped inputs from well-behaved function generators, one can observe deviations from linearity in the digitized output of an ADC channel. Deviation from the mean yields the differential nonlinearity (DNL) at the ADC channel [23]. Integration of the DNL yields the integral nonlinearity (INL) [23].

The measurement procedure makes use of two external function generators (Agilent 33220A) applied to the two differential inputs of a digitizer channel. The first function generator provides a slow ramp covering the full ADC range, while the second provides a faster ramp of smaller amplitude that modulates the signal from the first ramp. In our setup, the slow ramp waveform is set at 100% symmetry (sawtooth wave) with a period of 10 s and an amplitude of $\pm$1.25 V. The fast ramp waveform is set at 50% symmetry (triangle wave) with a period of 750 μs and an amplitude of $\pm$125 mV. Figure 1 shows a schematic plot of the two pulser outputs. These signals are summed together by the differential inputs of the digitizer.

A synchronized output of the function generator was used to externally trigger the digitization card on a rising or falling portion of the fast ramp. The digitized traces record a short, monotonic region of the fast ramp, as shown for example in Figure 2. The slope of the waveform is determined by the slope of the fast ramp, and its overall ADC offset is determined by the location along the slow ramp. For each sample within a waveform, a linear fit was performed within a 20 sample (δt = 200 ns) window, over which the fast ramp varies by roughly 1 ADC unit. Taking advantage of the small but finite high-frequency noise on the order of 1 ADC unit [24], the fit slope within each window provides a good measurement of the drop of the fast ramp in ADC units across the ADC channel nearest the center of the window.

Data was taken for about 30 minutes, corresponding to roughly 2.4M waveforms recorded on each digitizer channel, giving about 300000 fit slopes per ADC channel. We average the measurements for each ADC channel of a digitizer input to obtain that digitizer channel's final DNL curve, an example of which is shown in Fig. 3. As the slow ramp shifts the voltage offset of the fast ramp (the slow ramp's slope is much less than 1 ADC unit over the digitization window), each ADC channel is traversed by varying locations along the fast ramp. As a result, the DNL we compute averages over any nonlinearities of the fast ramp, making our method insensitive to imperfections in the fast ramp linearity. The computed averages also do not rely, as other nonlinearity measurements do, on the frequency with which a particular ADC channel is traversed, so that our method is also insensitive to nonlinearities in the slow ramp. These features enable the use of lower-cost function generators without stringent linearity specifications.

The measured DNL curve exhibits a picket-fence-like structure that is typical of multi-range ADCs. All digitizer channels measured show a similar trend with a similar magnitude, however the detailed structure and the sizes of the DNL spikes varied somewhat from one digitizer channel to the next,

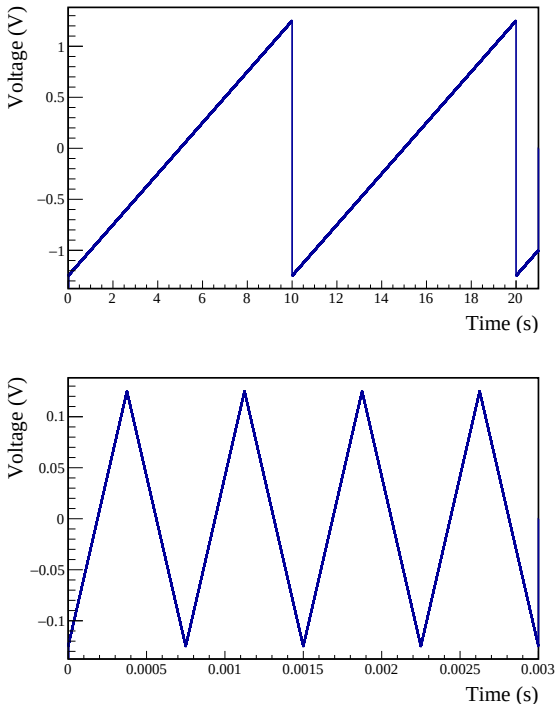

Fig. 1. Schematic plot for the external input: Top) slow ramp signals and Bottom) fast ramp.

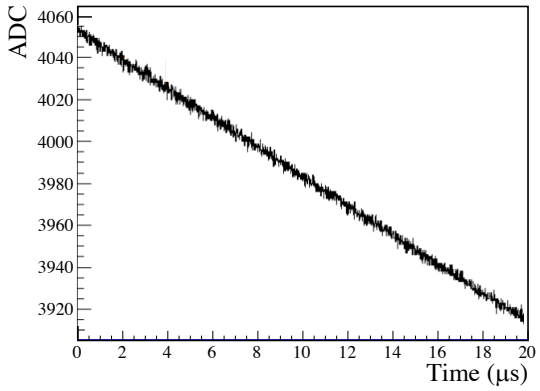

Fig. 2. Measured (down-going) waveform. A linear fit is performed within 20 samples (δt = 200 ns), over δADC $\sim$ 1 ADC unit.

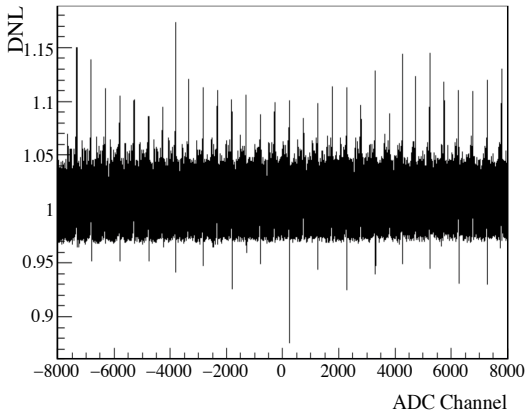

Fig. 3. An example measured average DNL curve at each ADC channel using high statistics data of a single digitizer channel.

requiring their individual measurement. For each digitizer channel, we integrate the measured DNL curve, and fit and subtract away any overall slope to obtain the INL curve, as shown for example in Fig. 4. The maximum deviation of the INL is at the level of approximately 2 ADC units, corresponding to about 1 keV (3 keV) for high gain (low gain) detector signals in the MAJORANA DEMONSTRATOR.

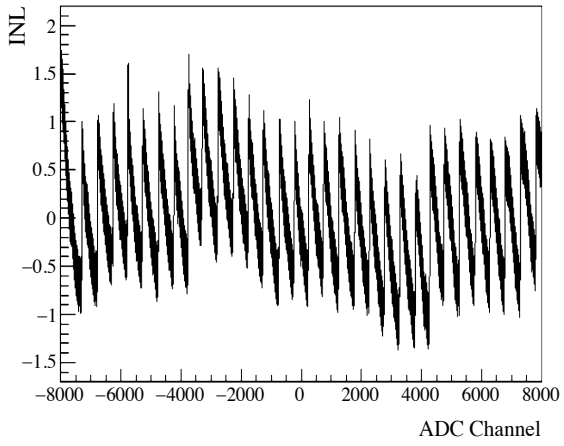

Fig. 4. An example measured INL curve for a single digitizer channel. The zig-zag pattern arises from the picket fence structure of the DNL curve.

Using this technique, we measured the INL with varying amplitude and trigger positions (up-going vs. down-going regions) of the fast ramp. The resulting ADC INLs exhibit hysteresis, particularly in the vicinity of the large DNL peaks (see Fig. 5). We interpret the hysteresis as a delayed response of the ADC to the signal. Using the slope of the fast ramp and the distance in ADC unit for the INL curves to come into agreement with each other following a large nonlinearity, we roughly estimated the time scale of the delayed response to be $\sim$1.4 μs. This time delay is incorporated into the nonlinearity correction described below. Our method was sufficient to reduce ADC nonlinearities to a negligible level, however the time delay could be optimized further with more careful study.

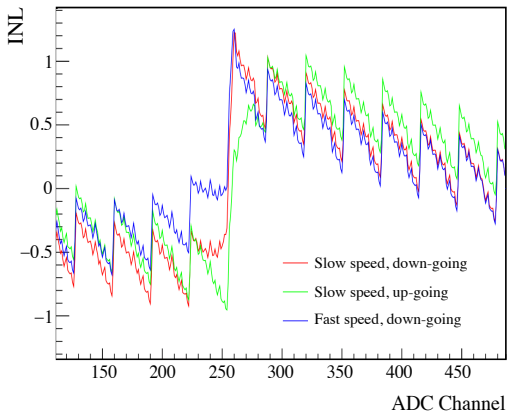

Fig. 5. An example INL curve over a small ADC range for different fast ramp amplitudes and directions. The ADC exhibits a hysteresis effect, which can be seen in both the measured INL curve deviation between opposite ramp directions (shown by the green and red curves) and in the larger deviation seen at higher ramp rates (seen in the difference between the red and blue curves at ADC values less than 260). The delayed response time constant describing the hysteresis effect is found from the number of ADC units needed for the curves to come into agreement following a large nonlinearity. The ramp rate is used to convert this value into a time.

III. NONLINEARITY CORRECTION

After searching for digitization problems such as range saturation or sticky ADC channels, recorded waveforms must be immediately corrected for nonlinearities, prior to further digital signal processing. To first order, our correction is applied using the INL curve as a look-up table. Additionally, a small recursive adjustment is made to correct the observed time delay in the ADC response.

First, we prepared estimates of the "instantaneous" INL curves in which the distortion due to the time delay was removed. This was accomplished by simply averaging the up-going and down-going curves. This inherently retains some of the distortion, but the remnant error was deemed to be negligible compared to other energy scale uncertainties and noise contributions. A more sophisticated treatment in which up-going and down-going measurements are spliced on either side of a large DNL spike, or in which a full deconvolution of the response time is performed, could yield improved performance.

Once the instantaneous INL curves are estimated, the nonlinearity correction is then applied. In the absence of the delayed response exemplified in Fig. 5, the correction would be applied by simply subtracting the INL from each ADC value. To account for the time delay, we instead compute

$$\mathrm{ADC}'_n = \mathrm{ADC}_n - \mathrm{INL}_{\mathrm{ref},n}, \tag{1}$$

where ADC'_n is the corrected ADC value of waveform sample n, ADC_n is its original ADC value, and $\mathrm{INL}_{\mathrm{ref},n}$ is a recursively computed reference correction that exponentially approaches the instantaneous INL value with time constant τ. It is given by

$$\mathrm{INL}_{\mathrm{ref},n} = \mathrm{INL}_{\mathrm{ref},n-1} + (\mathrm{INL}_n - \mathrm{INL}_{\mathrm{ref},n-1})\frac{\tau_s}{\tau}, \tag{2}$$

where INL_n is the instantaneous INL correction for sample n, and τ_s is the sampling period. The initial value of $\mathrm{INL}_{\mathrm{ref},n}$ is set to the INL of the average ADC value of a 1 μs region of baseline preceding the detector signal in the digitized trace. The value of τ is taken to be 1.4 μs for all digitizer channels; attempts to optimize this parameter channel-by-channel did not yield significant improvement in residual nonlinearities.

IV. Performance of the Nonlinearity Correction

The most straightforward and direct method to measure the performance of the nonlinearity correction is to compare energy calibration residuals before and after the correction is applied. Figure 6 shows such a comparison for ^{228}Th source data taken with the MAJORANA DEMONSTRATOR calibration system [25]. Since other sources of energy uncertainty are on the order of 0.1 keV [6], this comparison shows that without correction, ADC nonlinearity would be a dominant source of energy uncertainty in the MAJORANA DEMONSTRATOR. However, it does not provide a measure of the remnant contribution to the energy uncertainty of the ADC nonlinearity after applying our correction, because ADC nonlinearity is not the only source of variance in the data. Thus other methods are required to measure the performance of the correction in more detail.

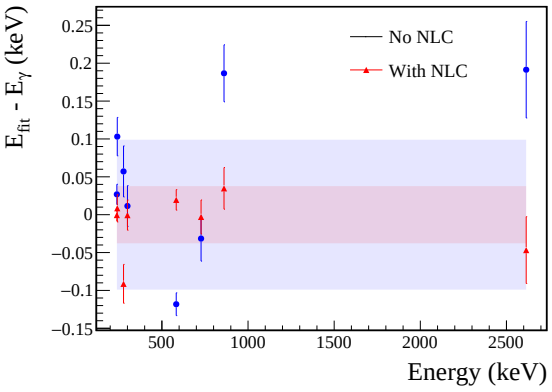

Fig. 6. An example of calibrated energy residuals in the high-gain amplification output of one detector before (blue circles) and after (red triangles) the non-linearity correction. The shaded regions characterize the non-statistical spread of the data points.

Since low gain channels in the MAJORANA DEMONSTRATOR have ∼1/3 the gain of high gain channels, the nonlinearity has different amplitude and energy periodicity in the high and low gain channels. This allows one to use the energy difference between the low and high gains to investigate the nonlinearity. Figure 7 shows one example of the difference in energies recorded simultaneously by each gain for events collected during a ^{228}Th calibration source deployment. The uncorrected trend (blue) exhibits a superposition of sawtooth-shaped nonlinearities from the low gain (large amplitude, long period sawtooth) and high gain (small amplitude, short period sawtooth) channels. Both patterns begin to wash out at higher energies because the signal region in the tail that is integrated by the trapezoidal filter spans a broader range

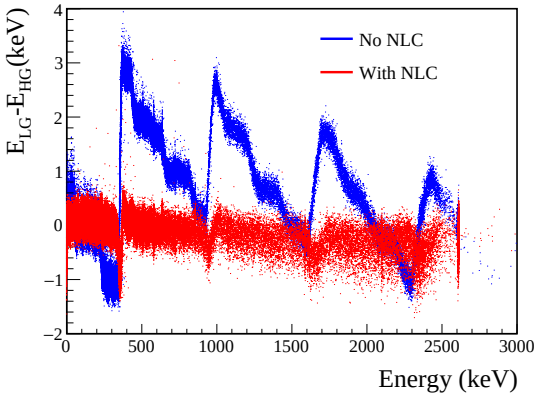

Fig. 7. The energy difference between the high gain and the low gain channels of ^{228}Th calibration source events for one detector. Blue dots show the energy difference prior to nonlinearity correction while red dots show the energy difference after our correction is applied.

of ADC channels, averaging away the nonlinearity. After correction (red trend), the energy difference is reduced by roughly an order of magnitude. The features in the remnant nonlinearity, including the overall slope and the appearance of small structures, vary subtly from channel to channel. However, based on the relative gains, on average the low gain contribution to the remnant nonlinearity should be roughly three times that from the high gain channel. The observed patterns are consistent with this estimate.

The front-end pulsers described in the introduction were also used to assess the ADC linearities over a limited dynamic range. First, a series of runs was taken in which the front-end pulser amplitude was stepped evenly over its full dynamic range, and the amplitudes of the output pulses were measured. The data were fit to a line, and the residuals were computed and calibrated into keV as estimates of the nonlinearities. With a single sweep one cannot distinguish ADC nonlinearities from potential nonlinearities in the pulser electronics themselves, so the observed nonlinearities in this first series of runs were taken as upper limits on the latter. Then a second set of runs was taken with the same series of pulser amplitude settings, except that the pulser signals were attenuated by a factor of ∼5 before being sent to the front-ends. The attenuators would shrink any nonlinearities inherent to the pulsers by the same factor; in our case, the observed nonlinearities in the second sweep were larger than those attributable to the pulser, and were consistent with being dominated by ADC nonlinearities. Figure 8 shows an example of nonlinearities derived from such pulser sweeps. While this method only covers a fraction of the energy range, it provides our best estimates of residual nonlinearities over that range. From these sweeps, we conclude that below ∼300 keV, remaining deviations from linearity are on the order of ±0.1-0.3 keV in all detectors in both cryostats, and are consistent with the more conservative method based on energy differences between low and high gain data that extends to much higher energies.

Finally, Figure 9 shows the impact of ADC nonlinearities and their correction in the delayed charge recovery (DCR)

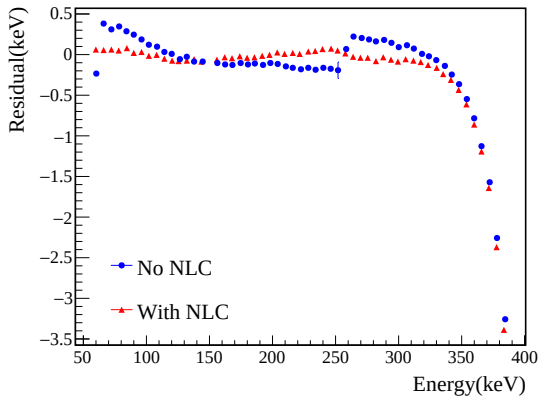

Fig. 8. Digitizer linearity as assessed via front-end pulser scans, with and without estimated energies corrected by the primary nonlinearity correction. The image displays residuals from a linear fit below 300 keV to the estimated energies of a sweep over attenuated pulser amplitudes. The deviation above ∼300 keV is due to saturation of the pulser dynamic range.

parameter used to reject events from alpha particles striking the passivated surface of the detectors [17]. Alphas incident on the passivated surface of the HPGe detectors exhibit significant charge trapping that is partially recovered at delayed times relative to the fast rise of their pulses. The ADC nonlinearity injects a visible wiggle in this parameter as a function of energy. Correcting for the nonlinearity significantly improves the DCR resolution and therefore the discrimination against alpha-incident events. The nonlinearity correction also drastically reduces the energy-dependence of the DCR cut signal acceptance.

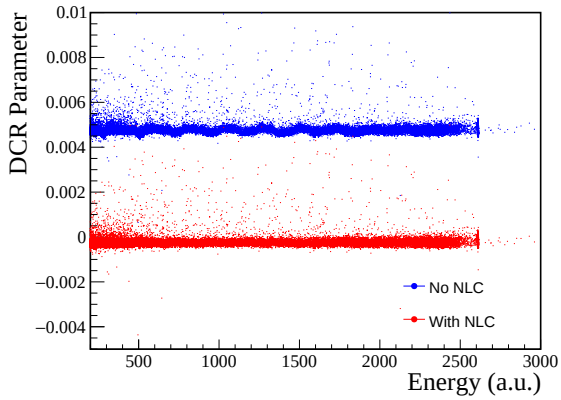

Fig. 9. ADC nonlinearities observed in the delayed charge recovery parameter for discriminating alphas, measured with calibration data in one detector. The blue dots show how the ADC nonlinearity injects a visible wiggle in the DCR parameter as a function of energy, while the red dots demonstrate how this variation is removed by the nonlinearity correction. An offset of the blue dots is added for better visualization.

V. Energy Systematic Uncertainty Quantification

Ultimately ADC nonlinearities cannot be completely eliminated, and their residual systematic effects must be characterized. In this final section, we describe the quantification of the contribution of residual ADC nonlinearities to the systematic uncertainty in event energy estimation in the MAJORANA DEMONSTRATOR. Systematic uncertainties in other pulse shape parameters can be estimated using similar techniques.

The impact of nonlinearities on energy estimation can be quantified in terms of their effect on the detector response function. In the MAJORANA DEMONSTRATOR this is particularly relevant, because the physics is extracted via the search for a peak at a known energy (the ^{76}Ge double-beta decay spectral endpoint, 2039 keV), with the shape of the response function. In the MAJORANA DEMONSTRATOR, as for many detectors, the peak shape is predominantly Gaussian, so that it is characterized essentially by just two parameters: the mean and RMS width. ADC nonlinearities modify both of these parameters. We compute the systematic uncertainties in these two parameters assuming an analysis in which events from all crystals are combined into a single distribution; biases for a crystal-by-crystal analysis can be computed using identical techniques.

The primary impact of ADC nonlinearities is an energy-dependent shift in the mean of the response function due directly to the value of the (residual) nonlinearity at any given energy. We refer to this as the "local" energy nonlinearity. We quantify the size of the local energy nonlinearities using the energy differences estimated between high and low gain channels, shown in Fig. 7. We divide the energy spectrum into fine energy bins so that the nonlinearity can be assumed to be constant over the bin. We then compute the average energy difference $\Delta_{LH}(E)$ between low and high gains in each bin for each detector. Since ADC nonlinearities are presumed to be a static property of the ADCs and since no evidence is observed for significant time variation of $\Delta_{LH}(E)$, possible time-dependent changes are ignored. Next, to accommodate our choice of an all-crystal analysis, we compute the average ($\overline{\Delta}_{LH}(E)$) and the RMS ($\sigma_{\Delta}(E)$) of these energy differences over all of the detectors in the array. The former biases the mean of the detector response, and the latter contributes to its width.

The energy variations in the $\Delta_{LH}(E)$ are observed to be roughly constant in scale across the entire energy spectrum. Since high gain channels in the MAJORANA DEMONSTRATOR have ∼3 times the gain of low gain channels, we assume that the relative residual nonlinearity at a given energy differ by a factor of 3 on average. Depending on the relative sign at each energy, these nonlinearities may add to or subtract from each other to give the observed $\overline{\Delta}_{LH}(E)$. We thus expect the residual non-linearities to lie within the ranges $\overline{\Delta}_{LH}/\left(1 \pm 3\right)$ for high gain channels, and $\overline{\Delta}_{LH}(E)/\left(1 \pm \frac{1}{3}\right)$ for low gain channels. We conservatively estimate the corresponding contributions to the systematic uncertainty in the detector response function mean to be $\frac{1}{2}\overline{\Delta}_{LH}(E)$ for high gain channels, and $\sqrt{1+\left(\frac{1}{3}\right)^2}\overline{\Delta}_{LH}(E)$ for low gain channels. The solid lines in Figure 10 shows the trend for $\frac{1}{2}\overline{\Delta}_{LH}(E)$ as a function of energy for all operating high gain channels using high-statistics calibration data with and without the nonlinearity correction applied. The energy uncertainty is highly suppressed by the nonlinearity correction and is below 0.1 keV over the full

calibration energy range.

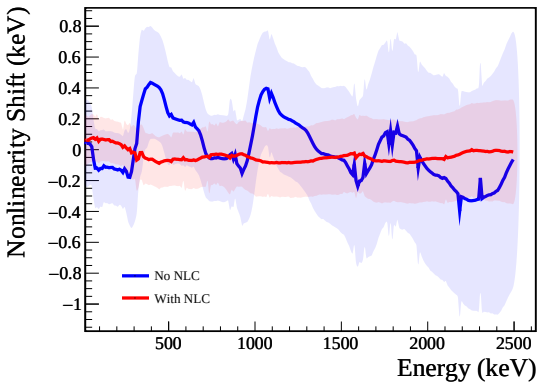

Fig. 10. Local energy systematic bias (solid line) and additional variance (shaded region) due to residual nonlinearities before and after the nonlinearity correction for all operating high gain channels using high-statistics calibration data.

In addition to shifting the mean, when events from multiple detectors are combined into a single spectrum, detector-to-detector differences in the local energy nonlinearities contribute to additional width in the combined, array-wide response function. Unfortunately, we cannot disentangle any difference in variability between the low gain and high gain nonlinearities from the data we have, so we conservatively take the full variability as an estimate of the resulting increase in the energy width for either gain. We thus inflate the width parameter of the energy response function by adding it in quadrature with $\sigma_\Delta(E)$ directly. The trend of $\sigma_\Delta(E)$ before and after nonlinearity correction is plotted as the shaded regions in Fig. 10. The width is substantially reduced by the correction, especially at higher energies, and is at the level of $\sim$0.2 keV over the entire energy range. The uncertainty contribution to the energy response function width due to the uncertainty in $\sigma_\Delta(E)$ is negligible compared to the Fano width.

In the MAJORANA DEMONSTRATOR and any similarly calibrated detector, nonlinearities also have a more global effect on the energy scale: the nonlinearities at the calibration points lead to non-statistical fit residuals (see Fig. 6), representing a possible pull in the entire calibration. Without a full model of the detailed energy dependence of the residual nonlinearities, this global energy bias can be bracketed with an additional systematic uncertainty in the mean of the detector response function. This contribution can be incorporated directly into the calibration fits by simply inflating the uncertainties in the calibration fit parameters by the square-root of the reduced χ^2 of the fit. This corresponds to adding an additional global variance at each calibration point that accounts for their non-statistical scatter about the best-fit curve. As can be seen from the scatter of the data points in Fig. 6, in the MAJORANA DEMONSTRATOR this contribution to the energy uncertainty is on the order of 0.05 keV.

VI. CONCLUSION

Nonlinearity is a well-known issue for fast ADCs. In this paper, we have shown this effect is observable in various aspects of MAJORANA DEMONSTRATOR data, including the energy difference between the low and high gains, the energy calibration residuals, and the delayed charge recovery pulse shape discrimination parameter. We have also demonstrated that the nonlinearity exhibits a non-trivial hysteresis and yet can be measured with inexpensive signal generators and corrected with simple, efficient algorithms. After the nonlinearity correction, the energy deviation from linearity is less than 0.1 keV, and the additional contribution to the energy width is about 0.2 keV. This correction was required to achieve the record energy resolution of the MAJORANA DEMONSTRATOR's neutrinoless double-beta decay search.

VII. ACKNOWLEDGEMENTS

This material is based upon work supported by the U.S. Department of Energy, Office of Science, Office of Nuclear Physics under contract / award numbers DE-AC02-05CH11231, DE-AC05-00OR22725, DE-AC05-76RL0130, DE-FG02-97ER41020, DE-FG02-97ER41033, DE-FG02-97ER41041, de-sc0012612, de-sc0014445, de-sc0018060, and LANLE9BW. We acknowledge support from the Particle Astrophysics Program and Nuclear Physics Program of the National Science Foundation through grant numbers MRI-0923142, PHY-1003399, PHY-1102292, PHY-1206314, PHY-1614611, PHY-1812409, and PHY-1812356. We gratefully acknowledge the support of the U.S. Department of Energy through the LANL/LDRD Program and through the PNNL/LDRD Program for this work. We acknowledge support from the Russian Foundation for Basic Research, grant No. 15-02-02919. We acknowledge the support of the Natural Sciences and Engineering Research Council of Canada, funding reference number SAPIN-2017-00023, and from the Canada Foundation for Innovation John R. Evans Leaders Fund. This research used resources provided by the Oak Ridge Leadership Computing Facility at Oak Ridge National Laboratory and by the National Energy Research Scientific Computing Center, a U.S. Department of Energy Office of Science User Facility. We thank our hosts and colleagues at the Sanford Underground Research Facility for their support.

REFERENCES

[1] N. Abgrall, E. Aguayo, F. T. Avignone III *et al.*, "The majorana demonstrator neutrinoless double-beta decay experiment," *Advances in High Energy Physics*, vol. 2014, p. 365432, 2014. [Online]. Available: https://www.hindawi.com/journals/ahep/2014/365432/

[2] P. Langacker and D. London, "Lepton-number violation and massless nonorthogonal neutrinos," *Phys. Rev. D*, vol. 38, pp. 907–916, Aug 1988. [Online]. Available: https://link.aps.org/doi/10.1103/PhysRevD.38.907

[3] N. Abgrall *et al.*, "New limits on bosonic dark matter, solar axions, pauli exclusion principle violation, and electron decay from the majorana demonstrator," *Phys. Rev. Lett.*, vol. 118, p. 161801, Apr 2017. [Online]. Available: https://link.aps.org/doi/10.1103/PhysRevLett.118.161801

[4] S. I. Alvis *et al.*, "First limit on the direct detection of lightly ionizing particles for electric charge as low as $e/1000$ with the majorana demonstrator," *Phys. Rev. Lett.*, vol. 120, p. 211804, May 2018. [Online]. Available: https://link.aps.org/doi/10.1103/PhysRevLett.120.211804

[5] C. E. Aalseth *et al.*, "Search for neutrinoless double-β decay in ^{76}Ge with the majorana demonstrator," *Phys. Rev. Lett.*, vol. 120, p. 132502, Mar 2018. [Online]. Available: https://link.aps.org/doi/10.1103/PhysRevLett.120.132502

[6] S. I. Alvis *et al.*, "A Search for Neutrinoless Double-Beta Decay in ^{76}Ge with 26 kg-yr of Exposure from the MAJORANA DEMONSTRATOR," *Phys. Rev. C*, vol. 100, no. 2, p. 025501, 2019.

[7] D. Doering, J. Joseph, H. Yaver, and S. Zimmermann, "Gretina digitizer specification," Gamma Ray Energy Tracking In-Beam Nuclear Array, Tech. Rep. GRT-3-060815-0, 2008. [Online]. Available: http://orca.physics.unc.edu/~markhowe/vme/Gretina4M_files/Gretina4Manual.pdf

[8] J. Anderson, R. Brito, D. Doering, T. Hayden, B. Holmes, J. Joseph, H. Yaver, and S. Zimmermann, "Data acquisition and trigger system of the gamma ray energy tracking in-beam nuclear array (gretina)," *IEEE Transactions on Nuclear Science*, vol. 56, no. 1, pp. 258–265, Feb 2009.

[9] J. Heise, "The sanford underground research facility at homestake," *Journal of Physics: Conference Series*, vol. 606, p. 012015, may 2015. [Online]. Available: https://doi.org/10.1088%2F1742-6596%2F606%2F1%2F012015

[10] P. N. Luke, F. S. Goulding, N. W. Madden, and R. H. Pehl, "Low capacitance large volume shaped-field germanium detector," *IEEE Transactions on Nuclear Science*, vol. 36, no. 1, pp. 926–930, Feb 1989.

[11] P. S. Barbeau, J. I. Collar, and O. Tench, "Large-mass ultralow noise germanium detectors: performance and applications in neutrino and astroparticle physics," *Journal of Cosmology and Astroparticle Physics*, vol. 2007, no. 09, p. 009, 2007. [Online]. Available: http://stacks.iop.org/1475-7516/2007/i=09/a=009

[12] S. Mertens, A. Hegai, D. Radford, N. Abgrall, Y.-D. Chan, R. Martin, A. Poon, and C. Schmitt, "Characterization of high purity germanium point contact detectors with low net impurity concentration," *Nuclear Instruments and Methods in Physics Research Section A: Accelerators, Spectrometers, Detectors and Associated Equipment*, vol. 921, p. 8188, Mar 2019. [Online]. Available: http://dx.doi.org/10.1016/j.nima.2018.09.012

[13] N. Abgrall *et al.*, "The majorana low-noise low-background front-end electronics," *Physics Procedia*, vol. 61, pp. 654 – 657, 2015, 13th International Conference on Topics in Astroparticle and Underground Physics, TAUP 2013. [Online]. Available: http://www.sciencedirect.com/science/article/pii/S1875389214006798

[14] M. A. Howe, G. A. Cox, P. J. Harvey, F. McGirt, K. Rielage, J. F. Wilkerson, and J. M. Wouters, "Sudbury neutrino observatory neutral current detector acquisition software overview," *IEEE Transactions on Nuclear Science*, vol. 51, no. 3, pp. 878–883, June 2004.

[15] S. I. Alvis *et al.*, "Charge trapping correction and energy performance of MAJORANA DEMONSTRATOR," in preparation.

[16] S. I. Alvis *et al.*, "Multisite event discrimination for the MAJORANA DEMONSTRATOR," *Phys. Rev. C*, vol. 99, no. 6, p. 065501, 2019.

[17] J. Gruszko *et al.*, "Delayed charge recovery discrimination of passivated surface alpha events in p-type point-contact detectors," *Journal of Physics: Conference Series*, vol. 888, no. 1, p. 012079, 2017. [Online]. Available: http://stacks.iop.org/1742-6596/888/i=1/a=012079

[18] D. Dallet and J. Machado da Silva, *Dynamic Characterisation of Analogue-to-Digital Converters*. Springer, 2005.

[19] T. E. Linnenbrink, S. J. Tilden, and M. T. Miller, "Adc testing with ieee std 1241-2000," in *IMTC 2001. Proceedings of the 18th IEEE Instrumentation and Measurement Technology Conference. Rediscovering Measurement in the Age of Informatics (Cat. No.01CH 37188)*, vol. 3, 2001, pp. 1986–1991 vol.3.

[20] P. Suchanek, D. Slepicka, and V. Haasz, "Several approaches to adc transfer function approximation and their application for adc non-linearity correction," *Metrology and Measurement Systems*, vol. 15, no. 4, pp. 501–511, 2008. [Online]. Available: http://www.metrology.pg.gda.pl/full/2008/M&MS_2008_501.pdf

[21] P. Suchanek, V. Haasz, and D. Slepicka, "Adc nonlinearity correction based on inl(n) approximations," in *2009 IEEE International Workshop on Intelligent Data Acquisition and Advanced Computing Systems: Technology and Applications*, Sept 2009, pp. 137–140.

[22] M. Gande, H. Venkatram, H. Y. Lee, J. Guerber, and U. K. Moon, "Blind calibration algorithm for nonlinearity correction based on selective sampling," *IEEE Journal of Solid-State Circuits*, vol. 49, no. 8, pp. 1715–1724, Aug 2014.

[23] T. C. Carusone, D. Johns, and K. W. Martin, *Analog Integrated Circuit Design*. John Wiley & Sons Inc., 2011.

[24] J. Potzick, "Noise averaging and measurement resolution (or "a little noise is a good thing")," *Review of Scientific Instruments*, vol. 70, no. 4, pp. 2038–2040, 1999. [Online]. Available: https://doi.org/10.1063/1.1149735

[25] N. Abgrall *et al.*, "The majorana demonstrator calibration system," *Nuclear Instruments and Methods in Physics Research Section A: Accelerators, Spectrometers, Detectors and Associated Equipment*, vol. 872, pp. 16 – 22, 2017. [Online]. Available: https://www.sciencedirect.com/science/article/pii/S0168900217308501